Domain wall resistivity in epitaxial thin film microstructures

2001 J. Phys.: Condens. Matter 13 R461

(http://iopscience.iop.org/0953-8984/13/25/202)

INSTITUTE OF PHYSICS PUBLISHING JOURNAL OF PHYSICS: CONDENSED MATTER

J. Phys.: Condens. Matter **13** (2001) R461–R488 www.iop.org/Journals/cm PII: S0953-8984(01)03635-9

TOPICAL REVIEW

Domain wall resistivity in epitaxial thin film microstructures

A D Kent[1], J Yu[1], U Rüdiger[2] and S S P Parkin[3]

[1] Department of Physics, New York University, 4 Washington Place, New York, New York 10003, USA
[2] RWTH Aachen, II Physikalisches Institut, D-52056 Aachen, Germany
[3] IBM Almaden Research Center, San Jose, CA 95120, USA

Received 3 August 2000, in final form 25 January 2001

Abstract

This article reviews our recent experimental studies of domain wall (DW) resistivity in epitaxial transition metal ferromagnetic thin film microstructures with stripe domains. The results are presented and analysed in the context of models of DW scattering and conventional magnetoresistance (MR) effects in ferromagnetic metals. Microstructures of progressively higher magnetic anisotropy and thus smaller DW widths have been studied, including; bcc Fe, hcp Co and $L1_\circ$ FePt. The magnetic domain structure of these materials have been investigated using magnetic force microscopy and micromagnetic simulations. In Fe and Co the dominant sources of low-field MR are ferromagnetic resistivity anisotropy, due to both anisotropic MR (AMR) and the Lorentz MR. In Fe, at low temperature, a novel negative DW contribution to the MR has been found. Hcp Co microstructures show a greater resistivity for current perpendicular to DWs than for current parallel to DWs, that is consistent with a small (positive) DW resistivity and a Hall effect mechanism. High anisotropy $L1_\circ$ FePt microstructures show strong evidence for an intrinsic DW contribution to the resistivity. Related studies and future directions are also discussed.

(Some figures in this article are in colour only in the electronic version; see `www.iop.org`)

1. Introduction

Domain walls (DWs) are intriguing objects in ferromagnetic materials with electronic properties distinct from that of ferromagnetic domains. A DW is an interface between uniformly magnetized regions (domains) with different magnetization directions. The length scale over which the magnetization direction changes is determined by material parameters (the exchange and magnetic anisotropy energies) as well as the sample geometry. DW widths are typically in the 1 to 100 nm range. Early theoretical studies of the electronic properties of DWs were stimulated by magnetotransport experiments on single crystal Fe whiskers [1–3]. Starting from a multidomain state a small field was observed to erase the DWs and produce large changes in resistivity at low temperatures (a reduction of the resistivity by an order of magnitude at 4 K) [4]. More recently, the discovery of giant magnetoresistance (GMR) associated with

magnetic domain reorientation in metallic multilayers and better control of the characteristics of magnetic nanostructures has renewed interest in the electronic properties of DWs.

GMR occurs in ferromagnetic/non-magnetic layered metallic thin films and is linked fundamentally to the electron's spin degree of freedom [5,6]. The relative magnetic orientation of thin ferromagnetic layers, that is the domain structure, determines the spin dependent electronic structure and the rate of electron scattering. Resistance changes of up to 35% in 10 mT magnetic fields at room temperature have been observed in Co/Cu multilayers [7]. While many materials show large (or even colossal) MR, only few show MR per unit applied field of this order. For instance, this is many orders of magnitude larger than ordinary magnetoresistance in ferromagnetic metals due to the Lorentz force. It is also (at least) one order of magnitude larger than the anisotropic magnetoresistance (AMR) effect in ferromagnetic metals [8,9]. In GMR materials the direct ferromagnetic exchange interactions between magnetic layers is broken by non-magnetic metallic layers. The magnetic interfaces thus correspond to the chemical interfaces, and are sharp nearly on the atomic scale. By contrast, within a DW the material is (1) chemically homogeneous and (2) magnetization varies on a larger length scale—the domain wall width. These two factors distinguish the physics of electron transport through a DW interface from that of a magnetic interface in a metallic multilayer. Nevertheless, there are common features. For instance, in both instances the electron spin direction changes on crossing a magnetic interface. Thus, as in GMR, spin dependent electron transport effects are expected to be important to understanding the scattering of electrons by DWs. It is only in the last few years that this possibility has been discussed [10, 11] and studied in some detail theoretically [12–14].

In this article we review progress in experiments that have addressed the physics of electron transport through DWs in epitaxial transition metal ferromagnetic structure as well as other materials. Section 2 discusses general aspects of this problem, which include, the energetics of stripe domain formation, models of DW resistivity and conventional MR effects associated with magnetic domains. The next sections (sections 3, 4 and 5) present our experiments on Fe, Co, and FePt epitaxial thin films. This is followed by a brief discussion of other interesting structures and materials in which DW resistivity has been studied. We conclude with a summary and some perspectives.

2. Domains in ferromagnetic metals

Stripe domain materials are ideal for studies of DW resistivity because they can have a large density of DWs and domain orientation as well as the spacing can be varied systematically. Our approach has been to produce a controlled array of closely spaced DWs in stripes parallel or perpendicular to the current in a microfabricated epitaxial structure. An applied magnetic field is then used to erase the domain structure and the change in resistance is measured to infer the DW resistivity. The following sections discuss the formation of stripe domain structures, theoretical models of DW resistivity and domain resistivity, that is, resistivity and MR associated with conventional transport effects due to ferromagnetic domains. The interested reader will find greater detail in the references.

2.1. Stripe domains

Domains form in ferromagnetic materials to reduce the magnetic dipolar energy, at the cost of the ferromagnetic exchange and magnetic anisotropy energies [15]. In general the domain structure in zero field is determined by minimizing the sum of these energies, and will depend considerably on the size, shape, and type of magnetic material. Also, it should be noted, that

domain patterns found in materials are often non-equilibrium patterns that depend on sample history, temperature, and other factors.

Uniaxial magnetic material are an interesting and simple example in which the magnetization is favoured by anisotropy forces to lie along a particular axis (the easy axis), taken to be the z-axis. Sample surfaces perpendicular to this axis lead to a stripe domain pattern, in which the magnetization direction alternates along the $+z$ and $-z$ directions [16]. Figure 1 shows schematic illustrations of stripe domains. The field energy is minimized by this subdivision at the cost of the formation of DWs (exchange and magnetic anisotropy energies). The z-axis sample size is the dimension which sets the equilibrium domain sizes. In addition, as the 'bulk' domain size (a in figure 1) grows further domain subdivision (branching) near the surface lowers the energy [16, 17], leading to intricate surface domain patterns.

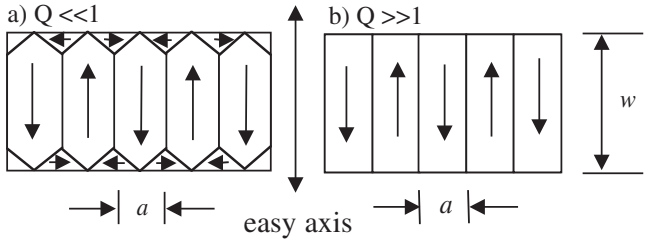

Figure 1. Illustration of stripe domain configurations in (a) low anisotropy ($Q \ll 1$) and (b) high anisotropy materials ($Q \gg 1$).

The domain configurations near sample boundaries are important to understanding the transport properties of stripe domain materials. Magnetic configurations at the sample boundaries are determined by the ratio of the anisotropy to magnetostatic energy, denoted by Q, $Q = K/2\pi M_s^2$. For small Q, $Q \ll 1$, flux closure domains $M \perp z$ are favoured to reduce the magnetostatic energy (figure 1(a)) , while for large Q, $Q \gg 1$, stripe domains which intersect the surface with $M \parallel z$ are favoured to reduce the magnetocrystalline energy (figure 1(b)). In the former limit minimization of the energy leads to a simple scaling in which the domain width goes as the square root of the z-axis sample dimension, w [18].

2.2. Domain wall resistivity

The first model of DW scattering was due to Cabrera and Falicov who considered the reflection of incoming electrons by the effective potential created by the rotating magnetization (and hence internal exchange field) within the wall [1]. The reflection probability was found to depend on the ratio of the DW width (δ) to the Fermi wavelength (λ), and be exponentially small for large ratios ($\sim e^{-\delta/\lambda}$). Thus for DWs in the 10 nanometer range and metals $\lambda_f = 0.1$ nm, the carrier reflection and hence the DW resistivity is entirely negligible.

The key ingredients in recent models of DW scattering are spin-dependent potentials and scattering rates, namely potentials and electron relaxation times that are different for majority (up) and minority (down) electrons in the ferromagnet. This, of course, is critical to our present understanding of GMR [5, 6]. It also significantly amplifies the effect of DWs on conductivity from that expected based on simple electron reflection from a DW. The basic idea is the following. In an uniformly magnetized ferromagnetic metal a large fraction of the total current is carried by one spin channel, either the majority or minority spins. Due to a small non-abiabaticity of the electron spin in traversing the wall, there is mixing of the spin channels within the DW [12]. This mixing partially elimimates the 'short circuit' provided

by the lower resistivity spin channel and increases the resistivity of the DW region. In a semiclassical Boltzmann calculation Levy and Zhang found that the MR for current parallel to the DW (CIW-current in wall) is:

$$R_{CIW} \equiv \frac{\rho_{CIW} - \rho_\circ}{\rho_\circ} = \frac{\xi^2}{5} \frac{(\rho_\circ^\uparrow - \rho_\circ^\downarrow)^2}{\rho_\circ^\uparrow \rho_\circ^\uparrow} \tag{1}$$

here the parameter $\xi = \hbar v_f/(J\delta)$ is a measure of the non-adiabaticity ($\xi = 0$ is an adiabatic crossing), where J the internal exchange energy, v_f is the Fermi velocity, δ is the DW width, and $\rho_\circ^{\uparrow(\downarrow)}$ is the resitivity of the spin up (down) channel. Physically, ξ is the ratio of the precession time of an electron in the exchange field to the time the electron takes to ballistically traverse the DW. In terms of length scales, this is the ratio of a 'spin precession length' to the DW width. The 'spin precession length' is the scale over which an electron at the Fermi energy completes a precession in the exchange field. Semiclassically, ξ is the angle a conduction electron spin makes with the local exchange field, the 'mistracking' discussed in [10, 11]. Clearly, as the wall region is narrowed the DW-MR is predicted to increase. It is also important to note that this is a perturbative result in ξ and thus the formula is not valid in the very narrow DW limit, such as an atomic scale DW. In this case the electron reflection would indeed be significant and MR effects greatly amplified [19]. Levy and Zhang further found that DWs cause larger MR when aligned perpendicular to the current flow (CPW-current perpendicular to wall).

$$R_{CPW} \equiv \frac{\rho_{CPW} - \rho_\circ}{\rho_\circ} = \frac{\xi^2}{5} \frac{(\rho_\circ^\uparrow - \rho_\circ^\downarrow)^2}{\rho_\circ^\uparrow \rho_\circ^\downarrow} \left(3 + \frac{10\sqrt{\rho_\circ^\uparrow \rho_\circ^\downarrow}}{\rho_\circ^\uparrow + \rho_\circ^\downarrow} \right) \tag{2}$$

Since the intrinsic reflection is assumed to be small (in contrast to CPP-GMR structures), spin accumulation effects are not taken into account here. Similar results have also been obtained by Brataas, Tatara, and Bauer, who considered both ballistic and diffusive transport through a DW [14]. For typical parameters for Co, $k_f = 10\,nm^{-1}$ and $J = 0.5$ eV, and $\rho_\circ^\uparrow/\rho_\circ^\downarrow = 5$, $\delta = 15$ nm, one finds a CPW-MR of 2%. Note that this is the MR of the DW material itself, and domains in a sample 'dilute' this MR contribution by the ratio of DW width to the domain size.

Interestingly, there are also models that predict an intrinsic negative DW contribution to the resistivity—that is DWs reduce the sample resistivity. Tatara and Fukuyama considered the effect of DWs on weak localization [13]. Weak localization is pronounced in low dimension disordered systems and arises due to quantum interference, which enhances electron backscattering and resistivity. Tatara and Fukuyama found that DWs destroy the electron coherence necessary for weak localization at low temperatures. As a consequence, in their model erasing DWs with a magnetic field restores weak localization and leads to an increase in the resistivity. The application of this model to Fe microstructures will be discussed in section 3.4.

A model by Gorkom, Brataas, and Bauer also found that DWs can be regions of enhanced conductivity, when the electronic structure of the DW is taken into account semiclassically [20]. The essential idea is that the effective exchange field within a DW is weakened due to the non-colinear spin alignment ($J \rightarrow J\cos(\theta)$, where θ is the angle between neighbouring spins). As a result, within a two band Stoner model of the ferromagnet, there will be a redistribution of charge among the majority and minority spin bands (i.e., a change in the sample magnetization within the DW). Depending on the relative relaxation times of the bands, this can produce a positive or negative DW contribution to the resistivity. They found that the magnitude of this effect can be the same order as those treated by Levy and Zhang.

2.3. Domain resistivity

The contribution of DWs to MR can be 'masked' by extrinsic MR associated with ferromagnetic domain configurations. There are three such effects we discuss below; ferromagnetic resistivity anisotropy, a Hall effect mechanism, and diamagnetic effects.

2.3.1. Ferromagnetic resistivity anisotropy It is well known that the resistivity of a ferromagnetic material depends on the angle of the sample magnetization and current [8, 9]. In addition, in a crystalline material the resistivity depends on the angle of the magnetization and crystal. At low temperature (well below T_c) there are two factors that contribute to this anisotropy; (1) anisotropic MR (AMR), which is due to spin–orbit coupling and (2) the Lorentz MR which depends on the angle of the current and internal field, B. These contributions will be discussed in more detail in the following sections.

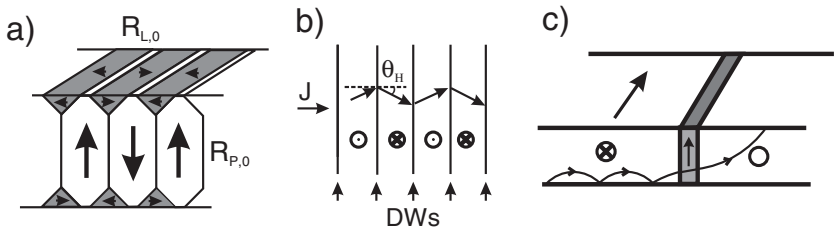

Figure 2. Stripe domain resistivity due to (a) ferromagnetic resistivity anisotropy, (b) a macroscopic Hall effect mechanism (view in the $z = 0$ plane), and (c) the orbital motion of charge near and in DWs.

In a multidomain sample, in which the magnetization is along more than one axis (figure 2(a)), saturating the magnetization with an applied field will produce changes in the angle of the current and magnetization in some parts of the sample, and hence a MR due to ferromagnetic resistivity anisotropy. For an uniaxial material in the small Q limit, domains at the border of the sample are parallel to the surface and perpendicular to the uniaxial axis (figure 1 (a)), as illustrated schematically in figure 2(a). Saturating this type of sample will produce a MR which reflects the difference in resistivity between perpendicular (indicated as, $R_{P,O}$) and longitudinally ($R_{L,O}$) oriented domains. In section 3 we discuss an effective medium model of the resistivity which can be used to estimate this MR.

2.3.2. Hall effect Berger showed that there is another extrinsic mechanism by which a multidomain sample may have a higher resistivity than a saturated sample. The mechanism is based on the Hall effect [3]. The Hall effect leads to an angle between the current and the electric field and in a ferromagnetic material the Hall angle can be large even in zero applied field due to the anomolous Hall effect, which is associated with spin–orbit effects [9, 21]. In a perpendicularly magnetized stripe domain material, in the CPW geometry, when the domain subdivision is smaller than the sample width, the Hall effect leads to current deflection near the DWs. In this geometry the electric field will be normal to the DWs, except in a narrow region (within about a domain width) of the sample boundaries. As the Hall angle changes sign in alternating magnetization domains, the current will zig-zag through the sample, as illustrated in figure 2(b). Berger found that this zig-zaging current leads to a resistivity increase of order $(\rho_{xy}/\rho_{xx})^2$, the Hall angle squared [21]. Also note that there is no such effect in CIW geometry, since in this case there is no current deflection. This means that there is a difference between CPW and CIW resistivities that goes as $(\rho_{xy}/\rho_{xx})^2$.

In the CPW geometry this also produces 'domain drag', a force which an electric current exerts on a DW. This force is due to the magnetic field generated by the zig-zagging current acting back on the domain structure. This effect has been observed in magneto-optic studies of perpendicularly magnetized current carrying wires [22].

2.3.3. Diamagnetic effects The orbital motion of charge near a DW has also been considered from a microscopic point of view, orginally by Cabrera and Falicov [2]. They found enhanced resistivity due to the 'convoluted zig-zag trajectories of charge near a wall.' This was also studied by Mankov, who found that the trajectories of charge near a wall can also lead to a decrease in the resistivity [23]. In both cases, these effects are of order $(\omega_c\tau)^2$, which can be large in very pure single crystals at low temperature but is generally small in metallic thin films.

In a thin film at low temperature the dominant electron scattering may occur at the film surfaces, a size effect originally considered by Fuchs and Sondheimer [24]. We have proposed a mechanism by which the interplay between this surface scattering and the electron orbital motion within domains may reduce the resistivity [25,26]. We considered a geometry in which the magnetization is in the film plane, as illustrated in figure 2(c). As shown, when diffuse electron scattering at the film top and bottom surface is important, the internal field acting on electron trajectories near walls will deflect charge from the film interfaces and reduce the amount of this scattering decreasing the film resistivity. We believe such an extrinsic effect may be relevant to understanding the experimental results on in-plane magnetized Fe thin films described in the next section.

3. (110) bcc Fe

The starting point for our DW scattering studies were high-quality (110) oriented bcc Fe films with thicknesses between 25 and 200 nm. The films were grown using seeded epitaxy in an UHV electron-beam evaporation system [26]. Figure 3 shows *in situ* low energy electron diffraction (LEED) and scanning tunnelling microscopy (STM) images of a Fe (110) film. The latter image shows the films are indeed very smooth, with large flat terraces separated by atomic steps. Magnetic shape anisotropy forces the magnetization to reside mainly in the film (110) plane which contains the easy [001], hard $[1\bar{1}1]$ and medium $[1\bar{1}0]$ magnetic axes. In this plane the magnetocrystalline anisotropy energy has a strong uniaxial component (2-fold) as well as a 4-fold component (for magnetic hysteresis measurements, see figure 1 of [27]). Strain in the film, due to a lattice mismatch with the substrate and epitaxial seed layer, serves to enhance this uniaxial component of the anisotropy [28].

3.1. Fe microstructures

These Fe films were patterned using optical lithography into transport wires (i.e. lines with a rectangular cross-section, given by the film thickness and pattern linewidth) for magnetotransport experiments. The wire long axis was aligned perpendicular to the [001] easy magnetic axis and parallel to the $[1\bar{1}0]$ direction. Figure 4 shows an example of a transport structure. The linewidth was varied between 0.5 μm and 20 μm and the distance between the voltage probes was 100 μm to 200 μm. A typical 100 nm thick Fe film had a residual resistivity ration (RRR) of 30 and a low-temperature resistivity of $\rho_0 = 0.2\ \mu\Omega$cm showing the high crystalline quality of the material [29]. An estimate of the electron mean free path at low temperature (4 K) is 200 nm, which is greater than the film thickness.

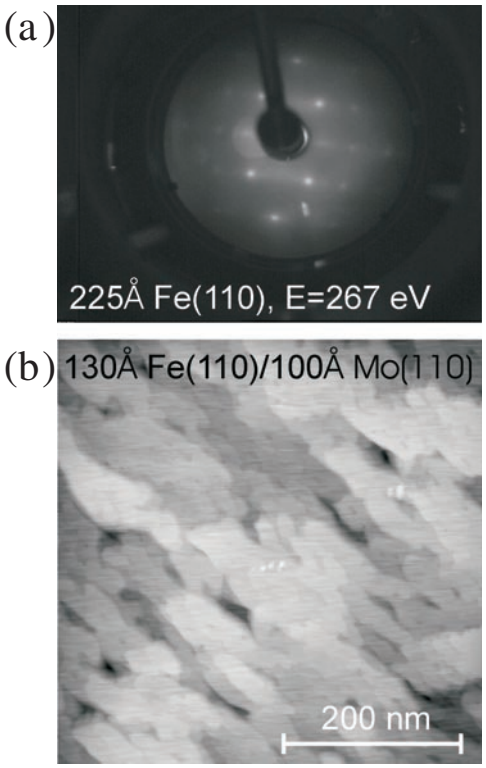

Figure 3. (110) bcc Fe film growth: (a) LEED image shows the expected two-fold symmetry of the surface and (b) STM shows elongated flat terraces separated by atomic steps.

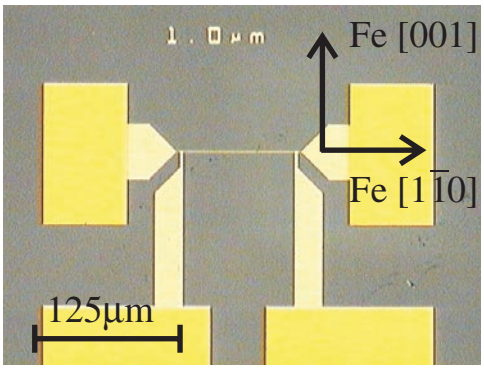

Figure 4. Optical micrograph of a 1 μm linewidth transport structure showing the Fe crystallographic directions.

3.2. Magnetic properties of (110) *Fe microstructures*

A competition between magnetocrystalline, exchange, and magnetostatic interactions in these wires leads to stripe domain configurations. Varying the linewidth changes the ratio of these energies and hence the domain size. Figure 5 shows magnetic force microscopy (MFM) experiments of microstructures of systematically varied linewidths in zero field performed at room temperature with a vertically magnetized tip. In these images the magnetic tip does not appear to change the domain structure. These images highlight magnetic poles at DWs and at the boundaries of the wires. Note that DWs appear either light or dark which is characteristic of Bloch walls, i.e. DWs in which the magnetization rotates out of the film plane producing magnetic surface charges [3]. Particularly evident in figure 5(b) is a tendency for alternating DWs to have the same sense of rotation or chirality, which further reduces the magnetostatic energy. White dotted lines in figure 5(a) illustrate the approximate domain structure. Images in the left-hand column were taken after the wire had been saturated transverse to its long axis, while those in the right hand column were taken after longitudinal magnetic saturation.

The domain size depends both on the wire linewidth and the magnetic history. The density of DWs varies by an order of magnitude for the linewidths investigated (0.5 μm to 20 μm)

[3] Note for films of this thickness asymmetric Bloch walls are expected, but would be difficult to detect with MFM. See reference [15], page 261.

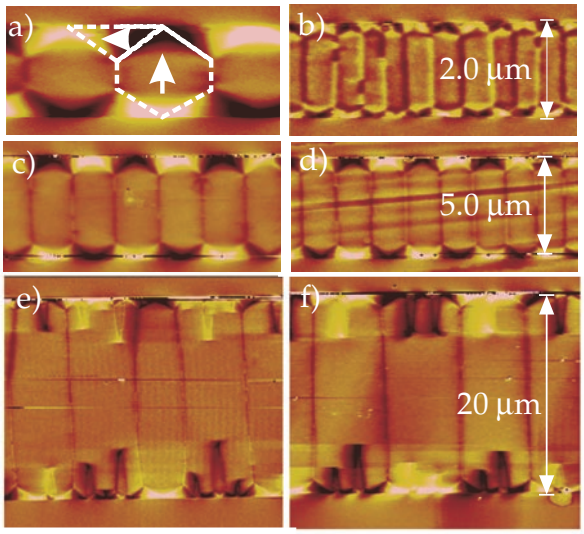

Figure 5. MFM images in zero applied field of (a),(b) 2 μm, (c),(d) 5 μm, and (e),(f) 20 μm linewidth Fe wires. Images in the left-hand column were taken after magnetic saturation transverse to the wire's long axis, while those in the right-hand column were taken after longitudinal saturation. The dashed lines in (a) illustrate the flux closure domain configuration observed.

and differences between domain configurations after transverse and longitudinal saturation are observed for wires with linewidths between 1 and 10 μm [29]. This latter effect is particularly dramatic in the 2μm wire (see figure 5 (a) and (b)) where the domain width varies by a factor of 4, from 0.45 μm after longitudinal saturation to 1.8 μm after transverse saturation. Equilibrium domain structures do not form because of energy barriers to domain nucleation and annihilation [27]. The magnetization reversal mechanisms have also been shown to depend on the magnetic field orientation using micromagnetic modelling [30]. The observed domain structure at $H = 0$ is stable over observation times of at least several hours showing that the DWs are strongly pinned at room temperature.

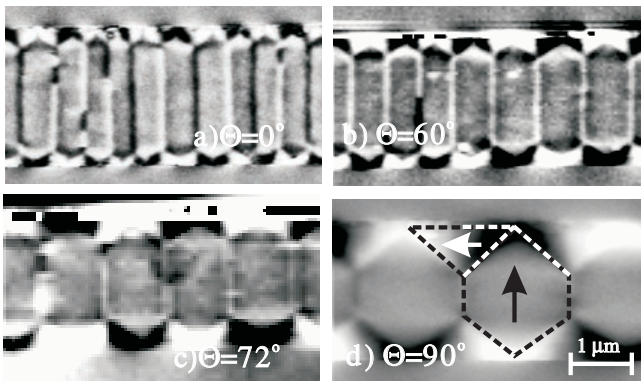

Figure 6. MFM images of the stripe domain pattern of a 2 μm Fe wire in zero field show a strong dependence on the previous saturation direction. Before performing the MFM images the wire was magnetized to saturation (a) longitudinal ($\Theta = 0^\circ$), (b) $\Theta = 60^\circ$, (c) $\Theta = 72^\circ$, and (d) transverse ($\Theta = 90^\circ$), with respect to the wire axis.

Interestingly this 'hysteresis' can be employed to systematically vary the domain structure in a single wire. This is illustrated by MFM images in figure 6 for a 2 μm linewidth wire. In these experiments the wire is first saturated with a large field at an angle Θ to the wire axis. The field is then reduced to zero at this angle and the domain structure examined with MFM. Figure 7 illustrates that the stripe domain width increases as the angle Θ between the saturating field and the wire axis is increased. In all samples closure domains of triangular shape are found near the wire edges. This is expected because the ratio of magnetocrystalline to magnetostatic energy is small for Fe, $Q = 0.03$.

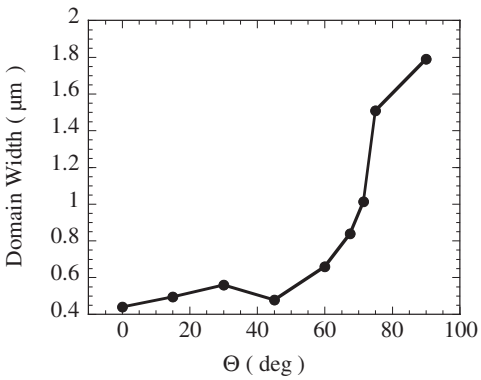

Figure 7. The domain width in zero field as a function of the saturation direction between the wire axis and the applied field, Θ.

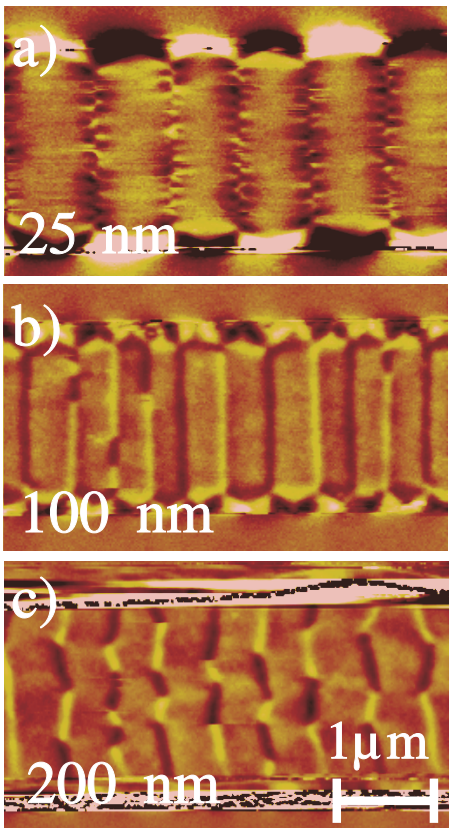

Figure 8. MFM images in zero field of a (a) 25 nm, (b) 100 nm, and (c) 200 nm thick Fe wire of 2 μm width after longitudinal saturation.

The wire thickness has also been used to systematically vary the domain structure. As the thickness is reduced the spin structure in the DWs change. This is shown in figure 8 for a 2 μm linewidth wire. In thin layers (25 nm) we find cross-tie walls (figure 8(a)). Whereas in thicker layers (200 nm) the DWs are Bloch walls and cant to bring sections of opposite chirality closer (figure 8(c)), reducing the magnetostatic energy at the cost of wall energy (greater exchange and anisotropy energies). As expected, the transition between these types of wall occurs when the film thickness is approximately the width of a DW in Fe $\sim$ 50 nm. The shape of these wires have been used to vary both the domain size and the DW spin structure for studies of electronic properties of DWs.

3.3. Magnetotransport properties of (110) *Fe microstructures*

Magnetotransport experiments were performed in a variable temperature high-field cryostat with *in situ* (low temperature) sample rotation capabilities. The applied field was in the plane of the film and oriented either longitudinal (∥) or transverse (⊥) to the wire axis. A four probe ac (∼10 Hz) resistance bridge with low-bias currents ($J < 10^4$ A cm^{-2}) was employed, and the magnetic history of the samples was carefully controlled.

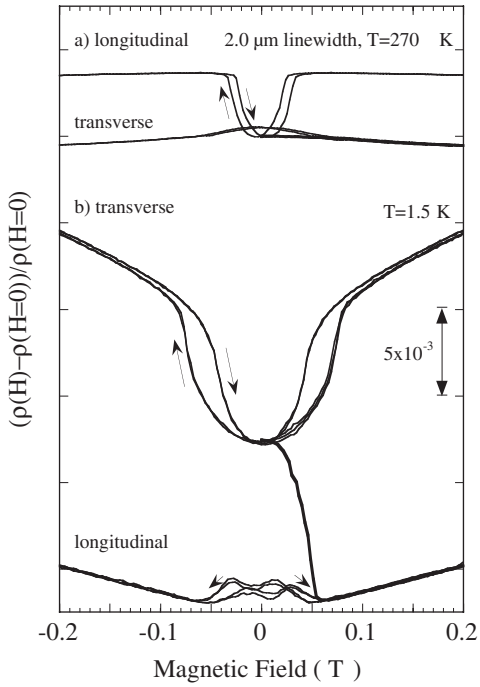

Figure 9. (a) MR data at 270 K of a 2 μm wire in the transverse and longitudinal field geometries ($\rho_\perp(H = 0$, 270 K)= 14.7 $\mu\Omega$cm). (b) MR at 1.5 K again in the transverse and longitudinal field geometries ($\rho_\perp(H = 0$, 1.5 K) = 0.74 $\mu\Omega$cm).

Figure 9 shows representative MR results on a 2 μm linewidth wire at both (a) high (270 K) and (b) low temperature (1.5 K) [29]. At 1.5 K there is structure to the MR in applied fields less than the saturation field $H_{s\parallel} = 0.035$ T and $H_{s\perp} = 0.085$ T, at which point the MR slope changes, and the resistivity then increases monotonically with field. An interesting feature of this data is that the resistivity anisotropy at high field changes sign with temperature. At 270 K the resistivity above the saturation field is larger in the longitudinal than in the transverse field orientation, while at 1.5 K this situation is reversed, $\rho_\perp(H_S) > \rho_\parallel(H_S)$.

This is due to two competing sources of resistivity anisotropy in these films, AMR and the Lorentz (or ordinary) MR. AMR has its origin in the spin–orbit interaction—the resistivity depends on the relative orientation of the magnetization and current [8,9]. Experimentally this anisotropy is determined by extrapolating the resistivity from a uniformly magnetized state, with the magnetization saturated in a particular direction relative to the current to zero internal field ($B = 0$), where the Lorentz force vanishes. The second effect is due to the ordinary (Lorentz) MR, or the curved trajectories of charge moving in a magnetic field. This is also, in general, anisotropic (i.e. dependent on relative orientation of J and B) [31]. As Fe has a large magnetization and hence a large internal magnetic field ($4\pi M = 2.2\ T$) both effects are of importance. The resistivity of domains parallel and perpendicular to the current direction can be written as:

$$\rho_\perp(B, T) = \rho_\perp(0, T)[1 + F_\perp(B/\rho_\perp(0, T))] \tag{3}$$

$$\rho_{\parallel}(B, T) = \rho_{\parallel}(0, T)[1 + F_{\parallel}(B/\rho_{\parallel}(0, T))]. \tag{4}$$

Here B is the internal field in the ferromagnet; $B = 4\pi M + H - H_d$, with H the applied field and H_d is the demagnetizing field. The AMR is equal to $[\rho_{\parallel}(0, T) - \rho_{\perp}(0, T)]/\rho(0, T)$, where $\rho(0, T)$ is the average resistivity. The function F is known as the Kohler function and parametrizes the Lorentz MR, for longitudinal and transverse field geometries in terms of $B/\rho \sim \omega_c\tau$, the cyclotron frequency times the relaxation time [24]. These scaling functions have been determined experimentally by performing MR measurements to large fields (6 T) as a function of temperature [31]. The scaling relationships are shown in figure 10. The inset displays both $\rho_{\parallel}(0, T)$ and $\rho_{\perp}(0, T)$ which result from this scaling analysis and which overlap on the scale shown. We find $\rho(0, T) \sim aT^2$ with $a = 3 \times 10^{-4} \mu\Omega\text{cm K}^{-2}$, as typically observed in 3d elemental ferromagnets. The AMR is $\sim 4 \times 10^{-3}$ above 80 K and decreases below this temperature. The reversal of the resistivity anisotropy at low temperatures ($\rho_{\perp}(H_s) > \rho_{\parallel}(H_s)$, figure 9(b)) is thus mainly a consequence of the increasing importance of the Lorentz MR (i.e., $F_{\perp} > F_{\parallel}$). At high temperature $\rho(0, T)$ is large and $F(x)_{x\to 0} \to 0$, so that the resistivity anisotropy is associated with the AMR as seen in figure 9(a) [9].

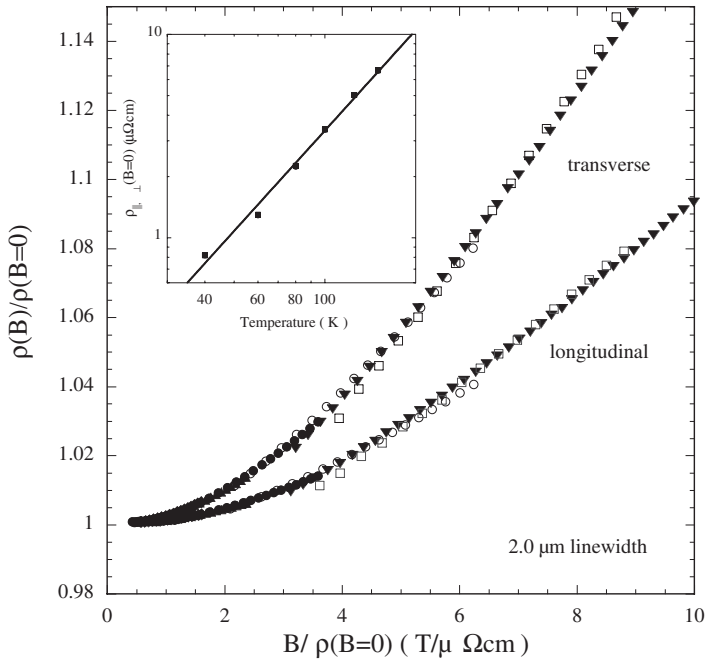

Figure 10. Scaling plot of transverse and longitudinal MR above magnetic saturation for a 2 μm wire in the form $\rho(B)/\rho(B = 0)$ versus $B/\rho(B = 0)$ at temperatures of (open squares) 1.5 K, (open triangles down) 40 K, (open circles) 60 K, (solid circles) 80 K, (solid triangles up) 100 K, (solid diamonds) 125 K, and (open diamonds) 150 K. The inset shows the scaling parameters $\rho_{\parallel}(B = 0)$ and $\rho_{\perp}(B = 0)$ as a function of temperature on a log-log plot, and overlap on the scale shown in the plot.

There are two ways we have estimated the DW contribution to the resistivity. The first was to perform MR measurements at the temperature at which the resistivity anisotropy at $H = 0$ vanishes. Since the AMR and the Lorentz MR contributions to the resistivity anisotropy are of opposite sign, there will be a temperature at which $\rho_{\parallel}(H = 0, T_{comp}) = \rho_{\perp}(H = 0, T_{comp})$,

which we denote the compensation temperature, T_{comp}. At this temperature the low-field MR due to the in-plane resistivity anisotropy approaches zero. Therefore, the remaining MR is due to DWs. A second method we have used enables one to extract the temperature dependence of the DW resistivity. We employ an effective medium model of the resistivty. The assumptions of this model are that (1) resisitivity anisotropy is small $((\rho_{\parallel}(B_i, T) - \rho_{\perp}(B_i, T)/\rho(B_i, T)) \ll 1$ and (2) the domain size is greater than the sample mean free path. We then can write the resistivity in the $H = 0$ magnetic state as:

$$\rho_{eff}(H = 0, T) = \gamma\rho_{\parallel}(B_i, T) + (1 - \gamma)\rho_{\perp}(B_i, T) \tag{5}$$

where γ is the volume fraction of domains oriented longitudinally (see figure 2 of [29]) and B_i is the field internal to these domains ($B_i = 4\pi M - H_d$). We determine $\rho_{\perp}(B_i, T)$ and $\rho_{\parallel}(B_i, T)$ by extrapolation of the MR data above saturation (again, as indicated by the dashed and solid lines in figure 11). The effective resistivity at $H = 0$ was estimated with the MFM measurements of γ. Deviations from this $\rho_d = \rho(H = 0) - \rho_{eff}(H = 0)$, i.e., the measured $H = 0$ resistivity minus this effective resistivity give the domain resistivity.

The compensation temperature for a 100 nm thick 2 μm linewidth wire is 65.5 K. MR

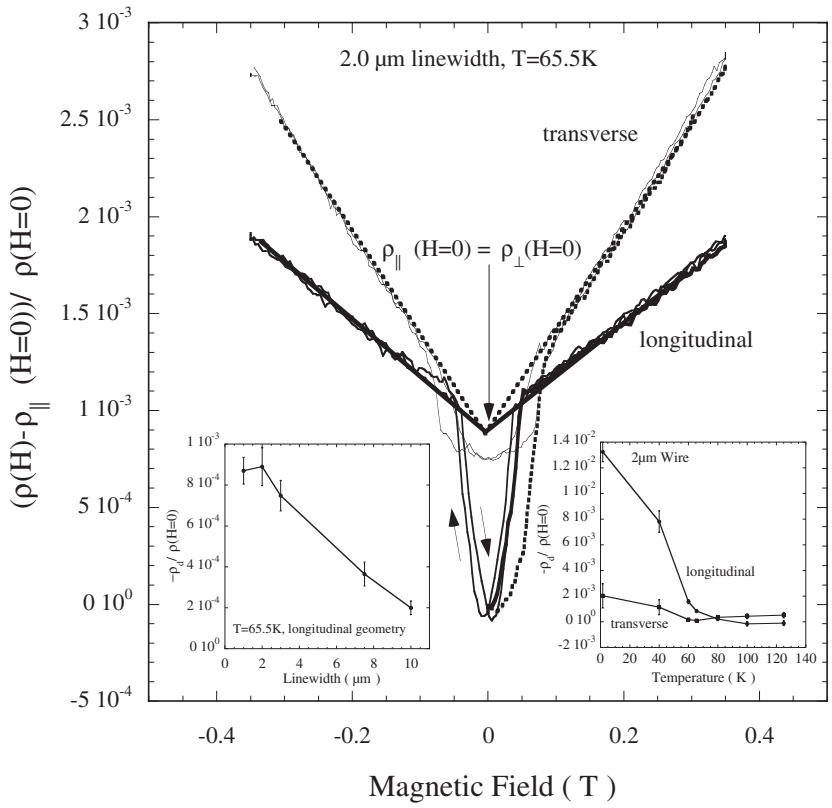

Figure 11. MR of a 2 μm Fe wire at 65.5 K. The extrapolation of the high-field MR data in transverse (dotted line) and longitudinal (solid line) geometry shows that $\rho_{\parallel}(H = 0) = \rho_{\perp}(H = 0)$. The resistivity with walls present, $\rho(H = 0)$, is smaller than this extrapolation and indicates that DWs lower the wire resistance. The left-hand inset shows this negative DW contribution as a function of linewidth at this compensation temperature in the longitudinal geometry. The right-hand inset shows the DW contribution as a function of temperature deduced using the model described in the text.

results at this temperature are shown in figure 11. The extrapolations of the high-field resistivity to $H = 0$ (dashed and solid line in figure 11) illustrate that the resistivity anisotropy approaches zero. However, the measured resistivity at $H = 0$ is lower in longitudinal than the transverse field orientation. This correlates with DW density, which is larger after longitudinal magnetic saturation (figure 5(a) and (b)). The magnitude of the effect also decreases systematically with increasing linewidth, (figure 11, left-hand inset) and, hence, decreasing DW density (figure 5(a) and(b)). The resistivity at $H = 0$ is suppressed when DWs are present in the wire. The domain structure of our samples has been determined at room temperature using MFM measurements. In order to determine the resistivity and MR starting from these domain configurations, we have also prepared the magnetic state of our samples at room temperature. To do this we warm up the sample to room temperature, cycle the magnetic field to establish a known $H = 0$ magnetic state, and cool again. The resistivity at $H = 0$ and the MR at low temperatures are unchanged for these samples in both longitudinal and transverse measurement geometries. This is strong evidence that the domain structure is not affected by temperature in this range and consistent with temperature dependent magnetic hysteresis loop measurements on wire arrays which show no change of the remanent magnetization with temperature.

The temperature dependence of the DW contribution to the resistivity has been estimated using the second method. The quantity ρ_d is negative and depends systematically on DW density, increasing in magnitude with increasing DW density (figure 11, left-hand inset). It approaches 1.3% of the wire resistivity at 1.5 K for a 2 μm linewidth wire (figure 11, right-hand inset). We also find that $|\rho_d|$ decreases with increasing temperature approaching zero at ~ 80 K (figure 11, right-hand inset). This enhancement of the conductivity vanishes at 80 K for all the wire linewidths investigated. Stated another way, the effective medium model accurately describes the $H = 0$ resistivity data on all wires above 80 K.

As shown previously in figure 7 and figure 8, the zero field stripe domain width can be varied continuously from 0.45 μm to 1.8 μm in a 2 μm linewidth wire by varying the angle of the sample and saturating field. We have used this to study the resistivity of a single wire as a function of the domain size [32, 33]. Figure 12 shows such measurements at 65.5 K, the compensation temperature. In these experiments the wire was first saturated with a field at an angle Θ to the wire axis, the field was then reduced to zero at this angle, and the wire reoriented into a transverse field geometry at $H = 0$. MR measurements were thus made in the transverse field geometry starting from the domain configuration established by this demagnetization procedure. The resistivity at $H = 0$ is smallest for $\Theta = 0$ and increases with increasing angle. This is shown in the inset of this figure for a larger set of angles. These results show that $-\rho_d/\rho(H = 0)$ increases with increasing DW density in a single wire, from 0.25×10^{-4} to 8×10^{-4} between the transverse ($\Theta = 90^\circ$) and longitudinal ($\Theta = 0^\circ$) orientations. This is an important demonstration that the reduction of the resistivity at $H = 0$ is associated entirely with a sample's domain configurations, since in this experiment the sample is otherwise unchanged, that is the sample has a constant cross-section, impurity configuration and defect structure.

Varying the film thickness changes both the DW spin structure (see figure 8) and the relative importance of bulk and thin film surface scattering on the resistivity of the wires. For the 2 μm linewidth wire the density of DWs does not change significantly with film thickness. Figure 13(a) and (b) present the MR of 100 nm and 200 nm thick 2 μm linewidth wires, respectively. Figure 13(a) shows that a positive MR is associated with the erasure of DWs in the 100 nm thick wire, and is largest in the longitudinal field geometry in which the DW density at $H = 0$ is greatest. By contrast, in the 200 nm thick wire the longitudinal MR is negative at low fields and positive at higher fields. This low-field negative MR is associated with a change in the magnetization reversal mode in thicker wires. The insets in figure 13 show MFM images of the magnetic structure in longitudinally applied fields at room temperature. In the 100 nm thick

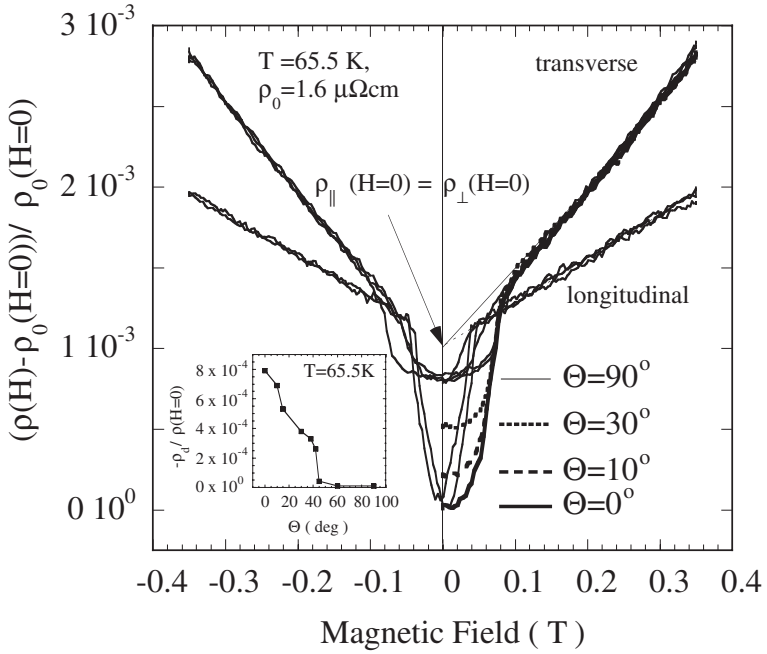

Figure 12. Low field MR of a 2 μm Fe wire ($\rho(H = 0, T = 65.5K) = 1.6\mu\Omega$cm) measured at the compensation point temperature of 65.5 K. Included are the MR data measured in transverse geometry from $H = 0$ to saturation after magnetizing the wire transverse ($\Theta = 90^\circ$), $\Theta = 30^\circ$, $\Theta = 10^\circ$, and longitudinal ($\Theta = 0^\circ$), with respect to the wire axis. The left-hand inset shows the reduction of resistivity $-\rho_d/\rho(H = 0)$ due to the presence of DWs as a function of Θ.

wire the reversal proceeds via the growth of favourably oriented longitudinal magnetized in-plane closure domains (inset figure 13(a)), whereas for the 200 nm thick film stripe domain configurations are observed (inset figure 13(b)). This latter image suggests that the magnetization has rotated out of the plane along {100} easy directions 45° to the surface normal. We suspect that there is a strong reduction in internal field (due to the strong demagnetizing fields perpendicular to the film plane) and this is responsible for the low-field drop in resistivity.

By establishing the magnetic state shown in figure 8(c) at room temperature by appropriate sample demagnetization and then cooling the sample to the MR measurement temperature (64.5 K), we find that the local maximum in the resistivity (longitudinal curve figure 13(b)) at $H = 0$ is associated with the canted DW structure (seen in figure 8(c)). Since the measured $H = 0$ resistivity is now observed to be equal to the $H = 0$ resistivity extrapolated from the high-field MR, ρ_d vanishes at this temperature for this wire. Table 1 summarizes the results of a systematic study of the effect of film thickness on ρ_d and the film resistivity. Even in thin layers (25 nm thick films), in which the DWs are considerably broader and Néel-like, there is a large anomalous negative DW contribution. In fact, the magnitude of the DW interface resistance (which is negative) and given by $r = \rho_d(d/\delta)\delta = \rho_d d$ where d is the domain size, is largest in thinner films ($\leqslant$ 100 nm).

3.4. Discussion of (110) Fe microstructure results

This observation of a negative DW contribution to the MR in Fe microstructures is a surprising result, and one that has been confirmed in experiments by another research group on similar

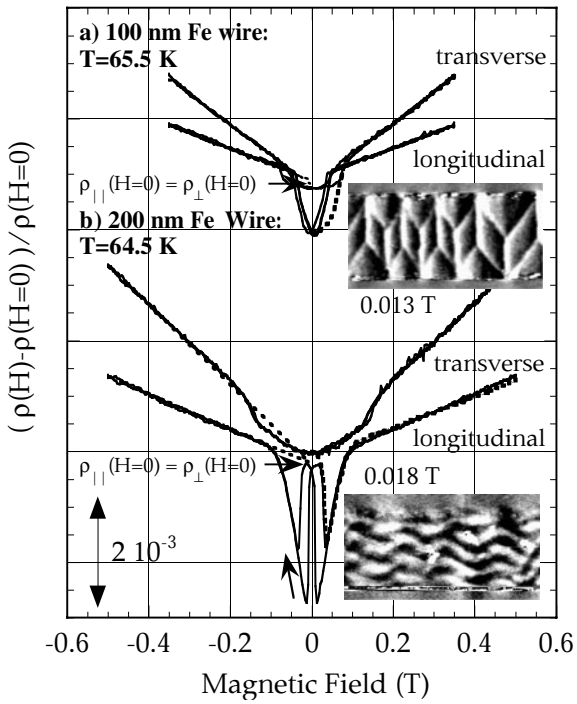

Figure 13. MR data at T = 65.5 K of (a) 100 nm and (b) 200 nm thick 2 μm linewidth Fe wires. The extrapolation of the high-field data shows $\rho_{\parallel}(H = 0) = \rho_{\perp}(H = 0)$, i.e. the absence of resistivity anisotropy.

Table 1. Characteristic data for 2 μm linewidth Fe wires of 25, 50, 100 and 200 nm thickness.

Thickness (nm)	25	50	100	200
ρ_0 (1.5 K) ($\mu\Omega$cm)	1.2	1.48	0.71	0.45
ρ_0 ($\sim$65 K) ($\mu\Omega$cm)	1.84	2.14	2.1	0.98
RRR	11.8	9.5	25.6	31.7
Domain size d (μm)	0.64	0.45	0.45	0.58
ρ_d/ρ_0 ($H = 0,\ T = 1.5$ K)	-0.5%	-0.75%	-1.2%	-0.6%
ρ_d/ρ_0 ($H = 0,\ T = 65$ K)	-0.06%	-0.1%	-0.1%	-0.0%
$r = \rho_d \times d$ (1.5 K) (Ωm^2)	-3.8×10^{-17}	-4.9×10^{-17}	-3.8×10^{-17}	-1.6×10^{-17}

materials [34]. As discussed in section 2.2 there are two models of DW resistivity that predict a reduction in resistivity. One is that of Tatara and Fukuyama based on weak localization (WL) phenomena [13]. They find that DWs contribute to the decoherence of conduction electrons which destroys WL. Essential to this model is the absence of other decoherence mechanisms, such as inelastic scattering. We have estimated the wall decoherence time from their model. On equating this with the inelastic scattering rate determined from measurements of the temperature dependence of the resistivity, we find the maximum temperature for WL phenomena is about 7 K [29]. On this basis the suppression of WL due to DWs cannot explain our observations of enhanced conductivity up to $\sim$ 80 K.

The second model of Gorkom, Brataas, and Bauer cannot be excluded as an explanation for our results. This model could be tested directly by conducting experiments on Fe microstructures with impurities which produce different asymmetries in the spin dependent scattering rates.

The fact that the negative DW contribution to the MR is not a strong function of the spin structure in the wall (see table 1) is an indication that the reduction in resistivity may

not be intrinsic to the DWs. We have proposed an extrinsic mechanism by which the alternating magnetization within the domains would increase the conductivity, that is illustrated in figure 2(c). The internal fields acting on charge near the DWs deflects charge away from the surface and reduce the amount of diffuse surface scattering. Increasing the film thickness acts to reduce the importance of surface scattering and hence this effect, as observed in experiment. For example, table 1 shows that in a 200 nm thick film the DW interface resistance, r, is reduced from that of thinner layers. This model could be tested by changing the nature of interface scattering, making it either more diffuse or specular. For instance, thin over- and underlayers have been shown to affect surface scattering in GMR structures [35, 36].

4. (0001) hcp Co

Hcp Co has a larger magnetocrystalline anisotropy, one order of magnitude larger than Fe, and hence DWs which are narrower than those in Fe by about a factor 3. Further, hcp Co has an uniaxial c-axis [0001] oriented magnetic anisotropy and with c-axis oriented thin films it is possible to achieve high densities of DWs. It thus appears that Co is the most promising of the elemental transition metals to show an intrinsic DW scattering contribution to the resistivity. In fact, in initial MR studies of such films 'large' negative MR for applied fields along the c-axis was interpreted as evidence of giant DW-MR [11]. We have shown that this is a misinterpretation of the data, and that this negative MR is actually a bulk effect linked to the domain structure in the interior of such films [37]. This interpretation is supported by detailed magnetotransport measurements, magnetic imaging and micromagnetic modelling studies, as described below. Nevertheless, such microstructures enable unique measurements of the difference between the CIW and CPW resistivities, as the DWs can be 'rotated' with an in-plane applied magnetic field.

4.1. Hcp Co microstructures

In perpendicularly magnetized thin films the film thickess is critical to determining the domain size. For this reason we have studied a series of microstructures of varied film thickness; 55, 70, 145, and 185 nm. The films were grown on a-axis $(11\bar{2}0)$ sapphire substrates with a thin Ru buffer (10 nm thick) and cap (5 nm, protective layer) using e-beam evaporation techniques, as described in [37]. X-ray $\Theta/2\Theta$ scans indicate c-axis orientation of the Ru and Co layers. Off-axis x-ray pole figures show that the films are also oriented in-plane with respect to the sapphire substrate. The films were then patterned using the same experimental procedures as discussed for the Fe samples. A residual resistivity of $\rho = 0.16\mu\Omega$cm and a residual resistivity ratio (RRR) of 19 for a 185 nm thick 5μm linewidth Co wire confirm the high crystalline quality of the films [4].

Figure 14 shows MFM images of a 70 nm thick 5 μm linewidth Co wire in zero magnetic field. These MFM images, taken with a vertically magnetized magnetic tip, highlight the out-of-plane component of the wire magnetization. Images were performed after magnetic saturation: (a) perpendicular to the film plane, (b) in plane and transverse to the wire axis, and (c) in plane and along the wire axis. As seen in figure 14, an in-plane applied field can be

[4] The measured room temperature resistivity of our hcp Co films is on average 3.3 $\mu\Omega$cm which is lower than the typical value for bulk hcp Co (5 to 6 $\mu\Omega$cm). This discrepancy may be associated with uncertainties in the dimensions of our wires. For example, due to the methods used to fabricate these samples (optical lithography and ion-milling) the uncertainty in wire thickness and width is approximately 20%. This leads to a 30% uncertainty in the wire resistivity. It is also possible that strain in the material changes the resistivity. This uncertainty in the absolute sample resistivity does not affect our analysis of the MR or the DW-MR.

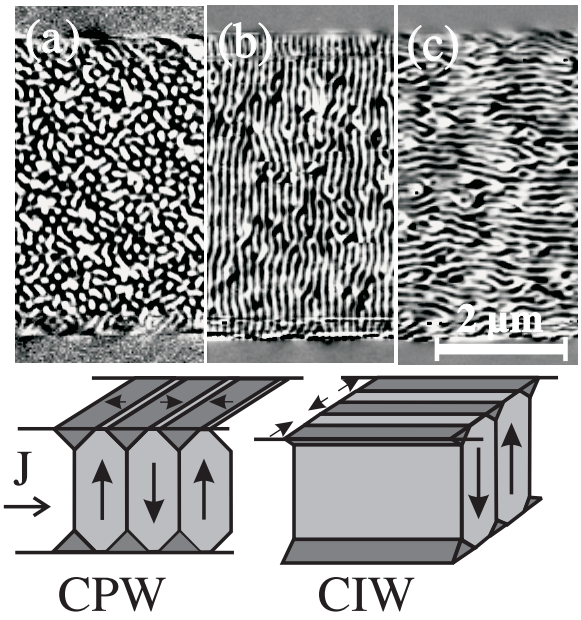

Figure 14. MFM images in zero applied field of a 5 μm linewidth 70 nm thick Co wire after (a) perpendicular, (b) transverse, and (c) longitudinal magnetic saturation. The model shows the orientation of stripe and flux closure caps with respect to the currents for (b) CPW and (c) CIW geometries.

employed to align DWs in parallel stripes [38]. Figure 14(b) and (c) show that DWs can be oriented parallel or perpendicular to the long axis of the wire and thus the applied current, the CIW and CPW geometries, respectively (as shown in the drawing in figure 14).

Modeling the micromagnetic structure of Co wires was essential to understand the MR results, particularly because hcp Co has an intermediate ratio of magnetocrystalline to magnetostatic energy, $Q = 0.35$. In fact, it has been shown by previous numerically modelling that in hcp Co DW's branch, being Bloch-like in the film center and forming flux closure caps at the top and bottom surface of the film to reduce the magnetostatic energy [39].

The magnetic structure of films of the thicknesses studied has been computed in zero field with the LLG Micromagnetics Simulator [40]. The equilibrium magnetization is found from the minimization of the system's free energy composed of exchange, magnetorystalline anisotropy, magnetostatic, and Zeeman terms. The time evolution of the magnetization is given by the Landau- Lifshitz-Gilbert equation [41]. The magnetization distribution is approximated by a discrete cubic mesh, with a volume of $10 \times 10 \times 10\,\mathrm{nm}^3$ per cubic mesh and tests performed with a finer grid have shown similar results. As seen in figure 15(a), such calculations produce domain widths which are in good agreement with experiment. The inset in figure 15(b) shows a part of the simulated magnetic cross section of a 70 nm thick Co element (with overall dimensions of $1500 \times 500 \times 70\,\mathrm{nm}^3$, where arrows indicate the magnetization direction of the stripes and the flux closure caps. Flux closure caps constitute approximately 25% of the total wire volume, which is also an approximate measure of the in-plane magnetized volume. For all Co wire thicknesses investigated the closure cap volumes (in-plane magnetization) were calculated as shown on the left-hand axis of figure 15(b). By increasing the wire thickness from 55 to 185 nm the in-plane magnetization volume decreases from 33 to 17%.

4.2. Magnetotransport properties of hcp Co microstructures

MR measurements were performed using the same experimental setup, discussed in the previous section. However, in this case three different orientations of the applied field were

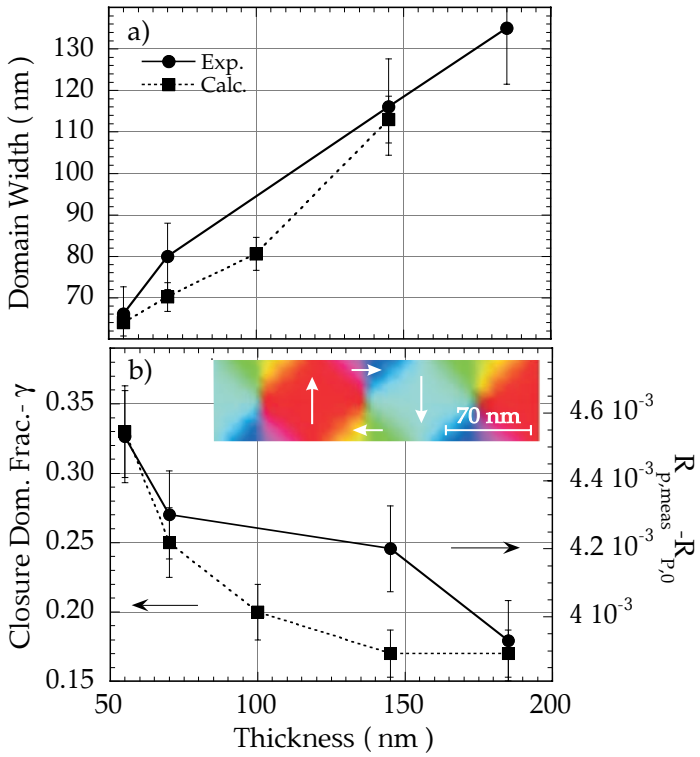

Figure 15. Domain size versus film thickness; experimental (solid circles) and calculated values (solid squares). (b) The calculated in-plane magnetization volume (solid squares) and the magnitude of the MR $R_{p,meas} - R_{P,0}$ in the perpendicular geometry (solid circles) as a function of wire thickness. Inset: Calculated magnetic domain cross section of a 70 nm thick Co element showing out-of-plane magnetized stripe domains and in-plane magnetized flux closure caps.

studied, the applied field (1) in-plane and perpendicular to the wire long axis (transverse), (2) in-plane and parallel to the wire long axis (longitudinal), and (3) perpendicular to the film plane (perpendicular).

The general features of the MR of these materials are very similar to those of the Fe microstructures. Figure 16(a) shows MR measurements performed at room temperature on a 55 nm thick film. The low-field MR is positive for in-plane magnetic fields and negative for perpendicular applied fields. Hysteresis is also evident, particularly in the perpendicular MR, which correlates well with the magnetization hysteresis loops (figure 17). Above the saturation field $\sim$ 1.4 T there is a large anisotropy of the resistivity, with the resistivity largest when the magnetization is in the film plane and parallel to the current (longitudinal geometry). Note that the resistivity is dependent on the relative orientation of M and J and the direction of M with respect to the crystal axes, with the resistivity smallest for M perpendicular to J and parallel to the [0001] direction (perpendicular geometry). At low temperature (1.5 K, figure 16 (c)) the resistivity is largest above the saturation field in the transverse geometry, with M perpendicular to J. As in the case of Fe, and for the reasons already discussed, the in-plane resistivity anisotropy changes sign with temperature.

Resistivity anisotropy is important in the interpretation of the low-field MR because the magnetization in zero applied field has components along all three dimensions. For example,

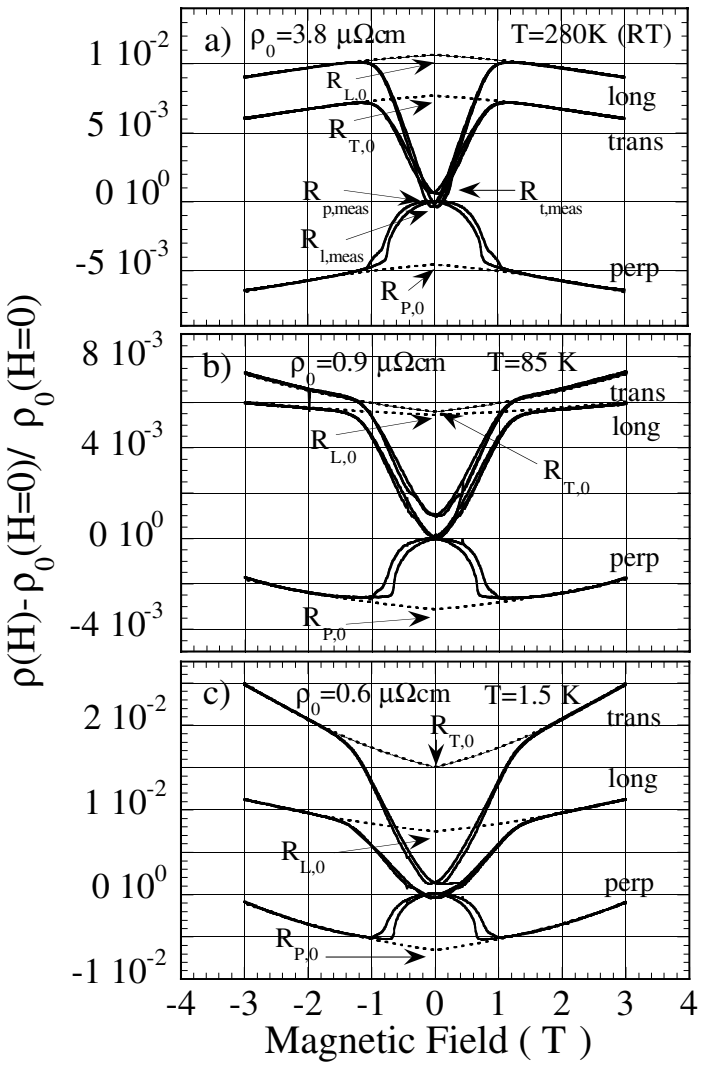

Figure 16. MR data of a 5 μm linewidth 55 nm thick Co wire in the perpendicular, transverse, and longitudinal geometry at (a) room temperature, (b) 85 K, and (c) 1.5 K.

for the CPW geometry (as illustrated in figure 14), the magnetization of the stripe domains are out-of-the film plane and perpendicular to the current. The magnetization of the flux closure caps are in-plane and parallel to the current, and the magnetization of the Bloch walls rotate through an orientation in-plane and perpendicular to the current. Thus a saturating field will both erase DWs and reorient the magnetization with respect to the current and crystal. The low-field MR which results from the resistivity anisotropy and the reorientation of the film magnetization was neglected in the initial work on hcp Co films, as it was incorrectly assumed that the magnetization and current remain always perpendicular in zero applied field [11].

This contribution can be estimated within an effective medium model of resistivity. To first order in the resistivity anisotropy, $\epsilon_L = R_{L,O} - R_{P,O}$ and $\epsilon_T = R_{T,O} - R_{P,O}$, the

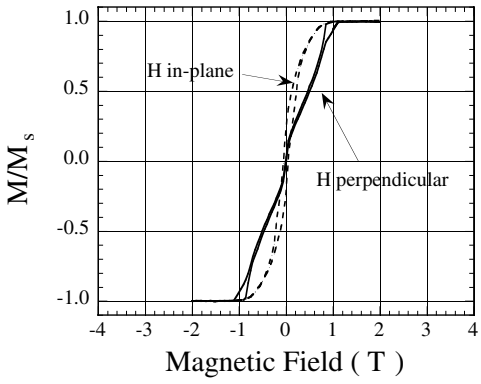

Figure 17. Magnetization hysteresis loops measured with a SQUID magnetometer of a 55 nm thick Co sample at 300 K for applied fields in-plane (dashed line) and perpendicular to the film plane (solid line).

perpendicular MR starting from the maze configuration (figure 13(a)) is:

$$R_{P,meas} - R_{P,0} = \gamma[1/2(R_{L,} + R_{T,0}) - R_{P,0}] + O(\epsilon_L^2, \epsilon_T^2), \tag{6}$$

where γ is the volume fraction of in-plane magnetized closure caps. Here $R_{L,T,P,O}$ are the MR values extrapolated from high field to $H = 0$ (dashed lines in figure 16), and normalized to the resistivity measured at $H = 0$ in the maze configuration, $\rho_o(H = 0)$ ($R_{P,meas}$ is taken to be the zero of the MR, see figure 16). The $H = 0$ resistivity has been determined by fitting the MR data above the saturation field to $aB^2 = a(4\pi M + H - H_d)^2$, with fitting parameter a, since the Lorentz MR must be an even functon of B. These fits and their extrapolation to $H = 0$ are shown in figure 16. In figure 16(b) it is seen that at $T_{comp} = 85$ K, the compensation temperature, the in-plane resistivity anisotropy ($R_{L,0} - R_{T,0}$) is nearly zero. In equation (6) the small volume of the in-plane magnetized DW material has been neglected, only the flux closure caps are considered. Within this picture, the negative MR observed in the perpendicular field geometry is due to the erasure of higher resistivity closure caps in the applied field. Further, the magnitude of the perpendicular MR is thickness dependent because the volume of the in-plane magnetized material depends on sample thickness (figure 15). For example, from the MR measurements performed at room temperature shown in figure 16(a) on a 55 nm thick film and with $\gamma = 0.33$, $R_{P,0}$, is estimated to be -4.5×10^{-3}, in close correspondence with the measured perpendicular MR. Figure 15(b) shows that the perpendicular MR generally increases with increasing in-plane magnetized volume fractions.

The differences between CPW and CIW resistivities (i.e., $R_{t,meas} - R_{l,meas}$) associated with rotating the magnetization direction of the flux closure caps from parallel (or antiparallel) to perpendicular to the current, in figure 16(a) is given in terms of the resistivity anisotropy by:

$$R_{t,meas} - R_{l,meas} = \gamma(R_{L,0} - R_{T,0}) \tag{7}$$

At 280 K this is 1×10^{-3}, in close agreement with the experimental value. Such estimates clearly illustrate that the main MR effects observed in this material are due to the film micromagnetic structure and resistivity anisotropy.

Temperature-dependent resistivity measurements for CPW and CIW geometries show behavior, which is not explicable simply in terms of ferromagnetic resistivity anisotropy. Equation (7) shows that the difference between CIP and CPW is proportional to the in-plane resistivity anisotropy. As this changes sign at low temperature, if the difference between CPW and CIW resistivities were only due to resistivity anisotropy it should change sign as well. Figure 18 shows that the measured, $\Delta_{tl} = R_{t,meas} - R_{l,meas}$ is always positive, while the resistivity anisotropy ($R_{L,0} - R_{T,0}$) is zero at about 85 K. At this temperature Δ_{tl} is 9×10^{-4}.

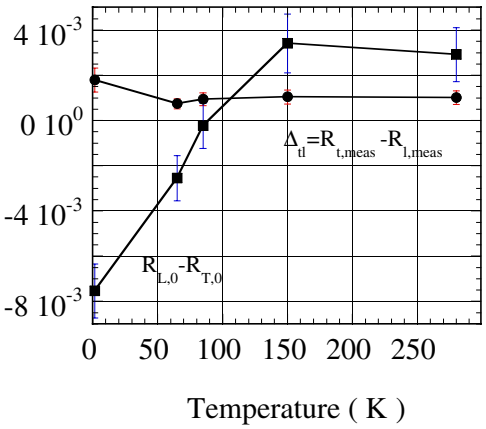

Figure 18. Temperature dependence of the difference between CPW and CIW resistivities, Δ_{tl}, and $R_{L,0} - R_{T,0}$ of a 55 nm thick Co wire.

4.3. Discussion of hcp Co microstructure results

The greater CPW resistivity is consistent with a small additional resistivity due to DW scattering, however, there is also another possible explanation for this result, which we discuss below. First, to get an idea of the order of magnitude of this possible DW scattering contribution to the resistivity, we assume that Δ_{tl} at T_{comp} is due to DW scattering. Since walls will be much more effective at increasing resistivity when arranged perpendicular to the current (compare equations (1) and (2)), we further assume DWs have only a small effect on resistivity when parallel to the current. The DW interface resistivity is then given by $r = (d/\delta)\Delta_{tl}\rho_0\delta = \Delta_{tl}\rho_0 d$, where d is the domain size, δ is the wall width ($\sim$ 15 nm) for hcp Co and ρ_0 is the film resistivity. Table 2 summarizes the MR measurements at the compensation temperature and these estimations for different wire thicknesses. For the films studied the average interface resistance is $6 \pm 2 \times 10^{-9}$ Ωm^2 at T_{comp} and the MR due to the DW material, $\Delta\rho_{wall}/\rho_0 = (d/\delta)\Delta_{tl}$, is 0.5%. For comparison, these values are approximately a factor of 100 smaller than the Co/Cu interface resistance and MR in GMR multilayers with current perpendicular to the plane of the layers [6].

Table 2. Characteristic data for 5 μm linewidth Co wires of 55, 70, 145 and 185 nm thickness.

Thickness (nm)	55	70	145	185
d (nm)	66	80	116	135
ρ_0 (1.5 K) ($\mu\Omega$cm)	0.63	0.26	0.23	0.16
ρ_0 (T_{comp}) ($\mu\Omega$cm)	0.92	0.68	0.58	0.3
ρ_0 (RT) ($\mu\Omega$cm)	3.38	3.04	3.31	3.04
Δ_{tl} (T_{comp})	0.94×10^{-3}	0.75×10^{-3}	1.3×10^{-3}	1.4×10^{-3}
$r(T_{comp})$ (Ωm^2)	5.7×10^{-19}	4.1×10^{-19}	8.7×10^{-19}	5.7×10^{-19}

Another mechanism that could produce the observed offset between CPW and CIW resistivities involves the Hall effect [3], discussed in section 2.3.2. This mechanism gives $R_{CPW} - R_{CIW} \approx (\rho_{xy}/\rho_{xx})^2$. While we have not measured this quantity we estimate this to be 4×10^{-4}, about half the observed difference.

5. (001) $L1_\circ$ FePt

Chemically ordered $L1_\circ$ FePt thin films have among the highest known magnetic anisotropy ($K \sim 10^8$ erg cm^{-3}) of any ferromagnetic material [42], about two orders of magnitude greater than hcp Co. This leads to DW widths of about 3 to 5 nm. This makes these materials of clear interest for studies of DW resistivity. We have studied (001) $L1_\circ$ FePt epitaxial microstructures with small scale stripe domains in which the degree of chemical order and hence the magnetic anisotropy has been varied by film growth conditions [43].

5.1. (001) *$L1_\circ$ FePt films*

Epitaxial (001) oriented $L1_\circ$ Fe_{1-x} Pt_x ($x \sim 0.5$) thin films (100 nm thick with thin Pt seed and cap layers) were grown by MBE in ultrahigh vacuum on (001) MgO substrates as described in [42]. The substrate temperature was varied between 150 and 500°C. X-ray diffraction analysis was used to determine the degree of chemical order (S/S_{max}) and film composition was determined by Rutherford backscattering (RBS) analysis [42]. The room temperature magnetic properties have been measured using both torque and vibrating sample magnetometry.

Domain structure was studied in zero applied field using MFM with vertically magnetized CoCr-coated Si tips. Prior to imaging, the films were demagnetized with a field applied perpendicular to the film plane. The light and dark contrast in the images is associated with magnetization parallel or antiparallel to the film normal. Figure 19 shows MFM images at room temperature of films (a) 1075 and (b) 1080. The average domain size is larger in the higher anisotropy film (1075, $\sim$ 200 nm). For film 1075 we estimate $Q = 10$. For such a large Q, stripe domains which intersect the surface with M perpendicular to the film surface are energetically favoured. Qualitatively larger anisotropy leads to a greater DW energy and hence larger domains, as observed in figure 19.

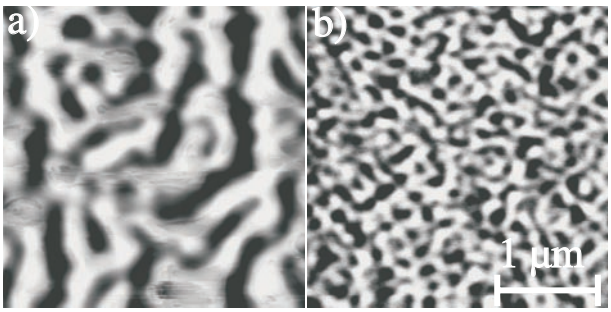

Figure 19. MFM images in zero applied field of $Fe_{1-x}Pt_x$ (a) 1075, a well ordered, high anisotropy film and (b) 1080, a less ordered lower anisotropy film.

Table 3 summarizes the properties of the films studied. With increasing substrate temperature there is a greater degree of chemical order and a higher uniaxial anisotropy constant. Torque measurements on samples 1079 and 1080, (and to a lesser extent on 1075) also indicate higher order components to the anisotropy, and that these films may be inhomogeneously ordered [44].

5.2. Magnetotransport properties of $L1_\circ$ FePt

The films were patterned using optical lithography and ion milling to produce 20 μm linewidth wires with contacts for measurement of both longitudinal and transverse (Hall) resistivities. The applied field was oriented perpendicular to the film plane (and current) as well as in the film plane and parallel to the current, denoted the longitudinal field geometry. Figure 20(a)

Table 3. Structural, magnetic, and transport characteristics of FePt films studied. δ is an estimate of the domain wall width ($\delta = \pi\sqrt{A/K_u}$, with $A = 10^{-6}$ erg cm^{-1}, d is the average domain size, ρ the resistivity and RRR is the residual resistivity ratio. Other symbols are as defined in the text.

Sample	T_g (°C)	x	S/S_{max}	M_s (emu cm^{-3})	K_U (10^7 erg cm^{-3})	δ (nm)	d (nm)	ρ ($\mu\Omega$cm) (1.7 K)	RRR	Domain MR (1.7 K)	$(\rho_{xy}/\rho_{xx})^2$ (1.7 K)
1075	500	0.49	0.80	834	4.30	4.4	210	7.2	3.0	2.8×10^{-3}	9.1×10^{-5}
1079	250	0.56	0.63	745	∼0.31	18	165	18.5	2.2	1.2×10^{-3}	3.1×10^{-4}
1080	150	0.51	0.47	837	∼0.28	19	90	26.6	1.8	1.1×10^{-3}	1.1×10^{-3}

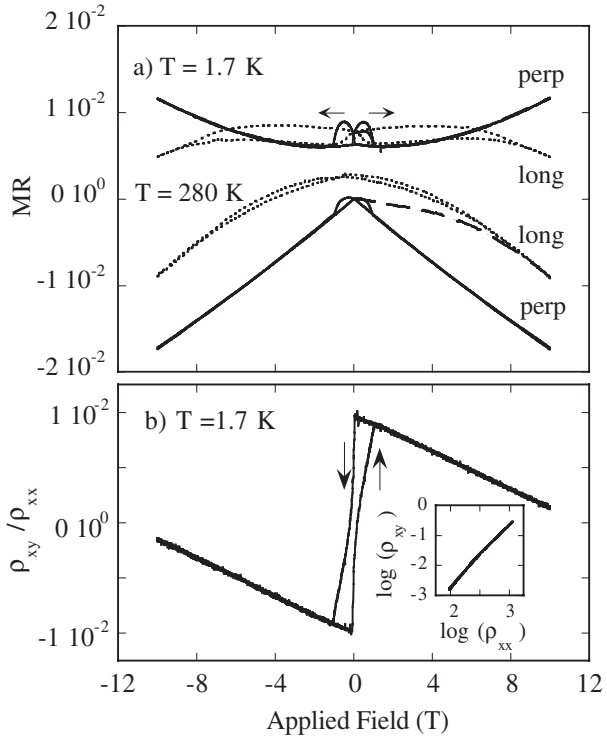

Figure 20. (a) MR data of a 20 μm linewidth wire of FePt 1075 at 1.7 K and 280 K. The solid line is with the applied field oriented perpendicular to the film plane and the dashed line is for the field oriented 5° from the film plane and parallel to the current. The field is purposely misaligned from the plane by this angle so that the sample is in a saturated magnetic state at high field. (b) The Hall angle, ρ_{xy}/ρ_{xx}, versus perpendicular applied field at 1.7 K. The inset in (b) shows a log–log plot ρ_{xy} versus ρ_{xx}.

shows MR measurements with the field oriented perpendicular (solid lines) to the film plane at 280 K and 1.7 K. In the low-field region MR hysteresis is observed which correlates well with magnetic hysteresis measurements. At low temperature, the high-field MR is positive and quadratic with field. This we associate with the ordinary (Lorentz) MR. At 280 K the high-field MR is negative and decreases nearly linearly out to the largest fields that we are able to apply (10 T). Such a negative MR is typically associated with the magnetic field suppression of spin-disorder scattering [9, 45].

Measurements in the longitudinal field geometry (with the field at 5° to the film plane) are indicated by dashed lines in figure 20. Resistivity anisotropy is noticeable at both high and low

temperatures. At low temperature (1.7 K) differences are observed particularly when magnetic domains are present, between −8 T and 8 T. At 280 K, the resistivity in the longitudinal geometry is generally larger than that in the perpendicular geometry. This is again associated with magnetic domain structure, which we discuss below.

Figure 20(b) shows the transverse or Hall resistivity as a function of field at 1.7 K. These characteristics are again hysteretic, reflecting the magnetic hysteresis. As commonly observed in ferromagnetic materials there is an ordinary linear high-field component and an extraordinary component proportional to the sample magnetization [9]. The extraordinary component is associated with the spin–orbit interaction, which leads to both asymmetric scattering (skew scattering) and a side-jump mechanism for the Hall effect. This latter contribution is predicted to scale as ρ_{xx}^2 [21]. The inset of figure 20(b) shows a log–log plot of ρ_{xy} versus ρ_{xx}. We observe $\rho_{xy} \sim \rho_{xx}^2$, consistent with the side-jump mechanism.

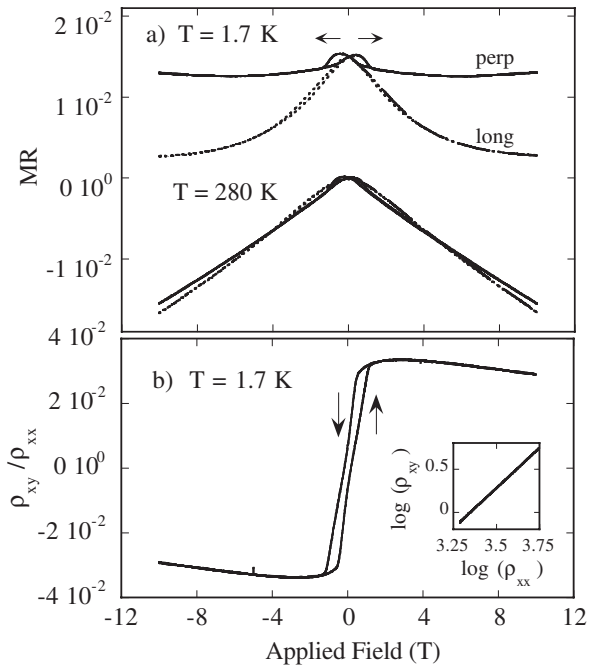

Figure 21. (a) MR data of a 20 μm linewidth wire of FePt 1080 at 1.7 K and 280 K in a perpendicular applied field. (b) The Hall angle versus perpendicular applied field at 1.7 K. The inset shows a log–log plot of ρ_{xy} versus ρ_{xx}.

Figure 21 shows similar magnetotransport measurements on a lower anisotropy film (1080) with greater chemical disorder. At the lowest temperature the resistivity is nearly field independent, and indicates a suppression of the Lorentz MR with increasing film disorder. At higher temperature a negative linear high-field MR is observed. Figure 21(b) shows that the extraordinary Hall angle is greatly enhanced with respect to that of 1075, consistent with the side jump mechanism ($\rho_{xy}/\rho_{xx} \sim \rho_{xx}$).

These magnetotransport results illustrate that domain structure has a significant effect on film resistivity in such materials. For instance, in film 1075, the resistivity is enhanced by 0.2% to 0.3% at low fields and temperatures due to the presence of magnetic domains. We denote this enhancement the domain MR. At 280 K a smaller enhancement in the resistivity is observed near zero field in the perpendicular MR. The larger resistivity in the longitudinal

geometry may be associated with the orientation of the domains. MFM imaging shows that after longitudinal measurements at 280 K, DWs tend to align perpendicular to the current, instead of in the maze-like pattern seen in figure 19. Low field enhancements in resistivity, somewhat smaller in magnitude (0.1%) are also observed in film 1080.

5.3. Discussion of $L1_\circ$ FePt results

An important question is the physical mechanism of this resistivity enhancement—whether it is due to an intrinsic DW scattering contribution to the resistivity or is an extrinsic domain effect. Most relevant in the latter case is the Hall effect mechanism discussed in section 2.3.2. In the high anisotropy film (1075), the Hall mechanism is of insufficent magnitude to explain the observed increase in resistivity. The observed increase in resistivity of 0.3% is more than one order of magnitude larger than $(\rho_{xy}/\rho_{xx})^2 \sim 0.01\%$ at 1.7 K. Also, while the Hall angle decreases as the temperature is reduced, the domain MR increases (figure 22). The ferromagnetic resistivity anisotropy is also not relevant, as $Q = 10$, the magnetization is largely perpendicular to the film plane and hence current. Further, the ferromagnetic resistivity anisotropy is small (figures 20 and 21). Film 1080 has a lower anisotropy, a smaller domain size and hence a larger density of DWs, yet the magnitude of the domain MR is reduced, $\sim$0.1%. In this film, $(\rho_{xy}/\rho_{xx})^2$ is also same order of magnitude and the Hall mechanism may be relevant.

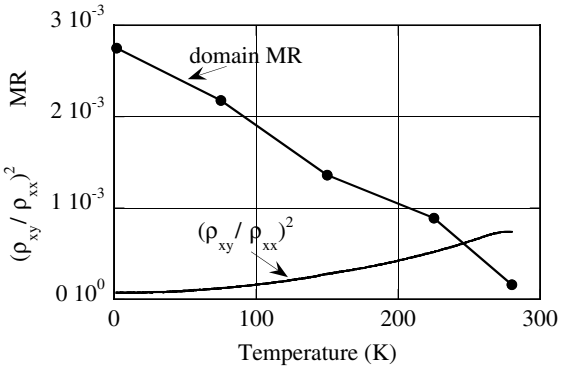

Figure 22. The domain MR and $(\rho_{xy}/\rho_{xx})^2$ versus temperature for sample 1075.

Thus in the highest anisotropy FePt film studied the low-field enhancement of the resistivity is consistent with an intrinsic spin dependent DW scattering contribution to the resistivity considered in [12, 14]. Since such DW scattering effects are predicted to depend strongly on the DW width, it would be interesting to extend such studies to even greater chemically ordered films, with higher anisotropy.

6. Other materials and structures

The study of DW resistivity has been an extremely active area of research in the last few years, with interest extending to oxide ferromagnetics, including double exchange systems, as well as other types of nanostructures [46–54]. First we note that other types of lithographic patterns and materials have been used to study DW resistivity in thin film transition metals. These include Co microstructures in which a zig-zag pattern was employed [47, 48]. This pattern results in DWs at corners due to magnetic shape anisotropy. Also, exchange-spring bilayers have been used to create a non-collinear spin structure in NiFe [46]. High anisotropy stripe domain materials, with somewhat lower anisotropy but otherwise similar to the those presented in section 5, have also been studied [55, 56].

Recently, experiments have been conducted on extremely narrow epitaxial hcp Co nanowires with one or two isolated head-to-head magnetization DWs [49]. These suggest a very large DW-MR. The wires were fabricated by electrodeposition in track etched membranes. For wires below approximately 35 nm, it was found that the hcp Co axis is parallel to the long axis of the Co wire. An MR of 0.6% was observed for an isolated DW in a wire about 1 μm in length. This is a large effect considering that the DW occupies a very small fraction of the wire. In fact considering this dilution the authors estimate a DW-MR of 100 to 600%, which does not make sense based on the expectations of DW-scattering models (equation (2), for instance). One must conclude that the DW is a significant scatterer and, based on our results, it must be significantly narrower in width than a DW in a Co thin film (15 nm). It has been suggested that the shape of the nanowire may in fact lead to a magnetic singularity (or Bloch point) in a head-to-head DW [15, 57]. This indeed could be a significant scatterer. If this is the case, it should be thought of as a barrier to transport, rather than a material in series with the magnetic domains in the wire, as the above estimation of the MR assumes. A natural explanation of this result is that fine (nearly atomic scale) micromagnetic structure is created in such a sample, which would lead to the spin acculumation suggested by the authors of [49]. However, the spin acculumation would be a consequence of strong reflection of electrons at the magnetic singularity rather than the origin of the MR. The DW structure would certainly be interesting to examine directly with a high resolution magnetic microscopy technique.

Studies of DW scattering in oxide ferromagnets have also recently been conducted. In the thin films of compressively strained $La_{0.7}Sr_{0.3}MnO_3$ with stripe domains. The main MR effects were understood in terms of bulk colossal MR and anisotropic MR [52]. There was also evidence for a small domain wall (DW) contribution to the MR, which was an order of magnitude larger than expected from a double exchange model [58]. In related experiments, a novel lithographic structure which uses small 'permanent' magnets close to a pattern of $La_{0.7}Sr_{0.3}MnO_3$ has been used to create DWs [53]. A small DW-MR was found which was, nonetheless, four orders of magnitude larger than expected from a simple double exchange picture.

Of particular note, a very clear indication of DW resistivity was recently obtained in epitaxial structures of the itinerant ferromagnet $SrRuO_3$ with stripe domains [54]. This material is also a 'bad metal', a material with an intrinsically small conductivity approaching values expected near a metal–insulator transition yet with a strong metallic temperature dependence of the conductivity. The films studied had an extremely high anisotropy $Q > 10$, and thus a well defined domain orientation. The DW interface resistance found was three orders of magnitude larger than what we reported for hcp Co in section 3.4. In addition, in these experiments the resistivity for both CPW and CIW was measured. Here a characterization of DW resistivity may lead to a better understanding of the mechanisms of transport in these unusual materials [59].

In a very recent development, evidence for very large MR in a ferromagnetic nanoconstriction has been presented [60]. This result has been interpreted in terms of DW scattering by an 'atomic' scale width DW trapped in the constriction region [19, 61, 62]. Certainly, further research is needed to clarify the mechanism of MR in such nanostructures.

7. Summary

Our studies of epitaxial thin film microstructures have eludicated the basic mechanisms of MR in transition metal ferromagnetic thin films with stripe domains. A close connection has been seen between magnetic microstructure and magnetotransport properties and, in particular, we have shown that magnetic imaging and micromagnetic simulations are essential to such studies. Characterization of the MR response to different field directions and to fields above

magnetic saturation field has also been important.

Our research has covered a range of materials, with progressively increasing magnetic anisotropy and narrower DWs. It is now clear in elemental thin film microstructures of Fe and Co DWs do not significantly scatter conduction electrons. The dominant sources of MR are ferromagnetic resistivity anisotropy, due to both the Lorentz MR and AMR. In Fe microstructures we have found a novel negative DW contribution to the MR which at present is not completely understood, but has been characterized in detail by experiments on films of varied thickness. In hcp Co microstructures temperature dependent magnetotransport measurements show that the CPW resistivity is always larger than the CIW resistivity. This is consistent with both DW scattering models as well as the Hall effect mechanism. In high-anisotropy thin films of $L1_{\circ}$ FePt evidence for an intrinsic DW scattering condition to the MR has been seen. It is the narrow DW width in this material, relative to a 'spin precession length', that appears to be critical to this observation (see, equation (1)).

In the last part we have summarized some of the very recent and exciting developments in this area. These new results and our experiments indicate that in samples with very narrow magnetic structure DW scattering can be a significant effect. In particular, in nanoconstrictions it has been suggested that the width of a DW will be characteristic of the size and shape of the constriction, rather than material characteristics [19]. Therefore, ferromagnetic nanoconstrictions may indeed have intrinsically large DW scattering effects, as recent results suggest [60, 62]. With the push to manipulating materials on the atomic scale it will soon be possible to conduct more systematic studies of mechanically stable atomic scale constrictions and perhaps create useful nanoscale MR devices which rely on magnetic DWs.

Acknowledgments

The authors are grateful for the outstanding collaborators who have made this work possible; Luc Thomas, Robin Farrow, Dieter Weller and Yuri Suzuki. We thank Peter Levy, Shufeng Zhang, Arne Brataas, and Luc Berger for interesting discussions and Neil Mathur for early preprints of his work. Our research was supported by DAPRA-ONR, Grant No N00014-96-1-1207. Microstructures were prepared at the Cornell Nanofabrication Facility (CNF). CNF is supported by the NSF under Grant ECS-9731293 and by its users, Cornell University and Industrial Affiliates.

References

[1] Cabrera G G and Falicov L M 1974 *Phys. Status Solidi* (b) **61** 59
[2] Cabrera G G and Falicov L M 1974 *Phys. Status Solidi* (b) **62** 217
[3] Berger L 1978 *J. Appl. Phys.* **49** 2156
[4] Taylor G R, Isin A and Coleman R V 1968 *Phys. Rev.* **165** 621
[5] Levy P M 1994 *Solid State Phys.* **47** 367
[6] Gijs M A M and Bauer G E W 1997 *Adv. Phys.* **46** 25
[7] Parkin S S P 1992 *Magnetic Surfaces, Thin Films and Multilayers* S S P Parkin, J-P Renard, T Shinjo and W Zinn (ed) p 211
[8] McGuire R and Potter R I 1975 *IEEE Trans. Magn.* **MAG-11** 1018
[9] Campbell I A and Fert A 1992 *Ferromagnetic Materials* E P Wohlfarth (ed) (Amsterdam: North-Holland) Vol 3
[10] Viret M, Vignoles D, Cole D, Coey J M D, Allen W, Daniel D S and Gregg J F 1996 *Phys. Rev.* B **53** 8464
[11] Gregg J F, Allen W, Ounadjela K, Viret M, Hehn M, Thompson S M and Coey M D J 1996 *Phys. Rev. Lett.* **77** 1580
[12] Levy P M and Zhang S 1997 *Phys. Rev. Lett.* **79** 5110
[13] Tatara G and Fukuyama H 1997 *Phys. Rev. Lett.* **78** 3773
[14] Brataas A, Tatara G and Bauer G E W 1999 *Phys. Rev.* B **60** 3406

[15] Hubert A and Schaefer R 1998 *Magnetic Domains* (New York: Springer)
[16] Landau L D, Lifshitz E M and Pitaevski L P 1984 *Electrodynamics of Continuous Media* (Oxford: Butterworth-Heinemenn)
[17] Choksi R, Kohn R V and Otto F 1999 *Comm. Math. Phys.* **201** 61
[18] Kittel C 1946 *Phys. Rev.* **70** 965
[19] For how an atomic scale DW can be formed, see:
Bruno P, 1999 *Phys. Rev. Lett.* **83** 2425
[20] van Gorkom R P, Brataas A and Bauer G E W 1999 *Phys. Rev. Lett.* **83** 4401
[21] Berger L 1970 *Phys. Rev.* B **2** 4559
[22] DeLuca J C, Gambino R J and Malozemoff A P 1978 *IEEE Trans. Magn.* **MAG-14** 500
[23] Mankov Y I, 1972 *Sov. Phys.-Solid State* **14** 62
[24] see, Ziman J M 1960 *Electrons and Phonons* (Oxford: Clarendon)
[25] Ruediger U, Yu J, Parkin S S P and Kent A D 1999 *J. Magn. Magn. Mater.* **198-199** 261
[26] Kent A D, Ruediger U, Yu J, Zhang S, Levy P M and Parkin S S P 1998 *IEEE Trans. Magn.* **34** 900
[27] Yu J, Ruediger U, Kent A D, Thomas L and Parkin S S P 1999 *Phys. Rev.* B **60** 7352
[28] Clemens B M, Osgood R, Pyne A P, Lairson B M, Brennan S, White R L, and Nix W D 1993 *J. Magn. Magn. Mater.* **121** 37
[29] Ruediger U, Yu J, Zhang S, Kent A D and Parkin S S P 1998 *Phys. Rev. Lett.* **80** 5639
[30] Thomas L, Parkin S S P, Yu J, Ruediger U and Kent A D 2000 *Appl. Phys. Lett.* **76** 766
[31] Schwerer F C and Silcox J 1968 *Phys. Rev. Lett.* **29** 101
[32] Ruediger U, Yu J, Kent A D and Parkin S S P 1998 *Appl. Phys. Lett.* **73** 1298
[33] Kent A D, Ruediger U, Yu J, Thomas L and Parkin S S P 1999 *J. Appl. Phys.* **85** 5243
[34] Kim S G, Otani Y, Fukamichi K, Yuasa S, Nyvlt M and Katayama T 1999 *J. Magn. Magn. Mater.* **198-199** 200
[35] Egelhoff W F *et al* 1997 *IEEE Trans. Magn.* **33** 3580
[36] Swagten H J M, Strijkers G J, Bitter R H J N, de Jonge W J M and Kools J C S 1998 *IEEE Trans. Magn.* **34** 948
[37] Ruediger U, Yu J, Thomas L, Parkin S S P and Kent A D 1999 *Phys. Rev.* B **59** 11914
[38] Kooy C and Enz U 1960 *Philips Res. Rep.* **15** 7
[39] Ebels U, Wigen P E and Ounadjela K 1998 *J. Magn. Magn. Mater.* **177-181** 1239
[40] Scheinfein M and Blue J L 1991 *J. Appl. Phys.* **69** 7740
[41] Aharoni A 1996 *Introduction to the Theory of Ferromagnetism* (Oxford: Clarendon)
[42] Farrow R F C, Weller D, Marks R F, Toney M F, Hom S, Harp G R and Cebollada A 1996 *Appl. Phys. Lett.* **69** 1166
[43] Yu J, Ruediger U, Kent A D, Farrow R F C, Marks R F, Weller D, Folks L, and Parkin S S P 2000 *J. Appl. Phys.* **87** 6854
[44] Farrow R F C, Weller D, Marks R F and Toney M F 1998 *J. Appl. Phys.* **84** 934
[45] Gerber A, Milner A, Korenblit I Y, Karpovsky M, Gladkikh A and Sulpice A 1999 *Phys. Rev.* B **57** 13667
[46] Mibu K, Nagahama T, Shinjo T and Ono T 1998 *Phys. Rev.* B **58** 6442
[47] Taniyama T, Nakatani I, Namikawa T and Yamazaki Y, 1999 *Phys. Rev. Lett.* **82** 2780
[48] Taniyama T, Nakatani I, Yakabe T and Yamazaki Y 2000 *Appl. Phys. Lett.* **76** 613
[49] Ebels U, Radulescu A, Henry Y, Piraux L and Ounadjela K 2000 *Phys. Rev. Lett.* **84** 983
[50] Wegrowe J-E, Comment A, Jaccard Y, Ansermet J-P, Dempsey N M and Nozieres J-P 2000 *Phys. Rev.* B **61** 12216
[51] Xu Y B *et al* 2000 *Phys. Rev.* B **61** R14901
[52] Wu Y, Suzuki Y, Ruediger U, Yu J, Kent A D, Nath T K and Eom C B 1999 *Appl. Phys. Lett.* **75** 2295
[53] Mathur N D *et al* 1999 *J. Appl. Phys.* **86** 6287
[54] Klein L, Kats Y, Marshall A F, Reiner J W, Geballe T H, Beasley M R, and Kapitulnik A 2000 *Phys. Rev. Lett.* **84** 6090
[55] Ravelosona D, Cebollada A, Briones F, Diaz-Paniagua C, Hidalgo M A and Batallan F 1999 *Phys. Rev.* B **59** 4322
[56] Viret M, Samson Y, Warin P, Marty A, Ott F, Sondergard E, Klein O and Fermon C 2000 *Phys. Rev. Lett.* **85** 3962
[57] Arrot T 2000 private communication
[58] Brey L 2000 preprint: /xxx.lanl.gov/cond-mat/9905209
[59] Klein L, Dodge J S, Ahn C H, Snyder G J, Geballe T H, Beasley M R, and Kapitulnik A 1996 *Phys. Rev. Lett.* **77** 2774
[60] Garcia N, Munoz M and Zhao Y W 1999 *Phys. Rev. Lett.* **76** 2923 .
[61] Tatara G, Zhao Y-W, Muoz M and Garcia N 1999 *Phys. Rev. Lett.* **83** 2030
[62] Garcia N, Munoz M and Zhao Y W 2000 *Appl. Phys. Lett.* **76** 2586